INTERACTION OF OFFSHORE SUPPORT VESSEL WITH ADJACENT OFFSHORE WIND TURBINE DURING MAINTENANCE OPERATION

Xiudi Ren[1,2,3]   **Longbin Tao**[3]   **Martin Nuernberg**[4]   **Iman Ramzapoor**[3,5]

1. Key Laboratory of Far-shore Wind Power Technology of Zhejiang Province. Hangzhou, Zhejiang, China.
2. PowerChina Huadong Engineering Corporation Limited. Hangzhou, Zhejiang, China.
3. Department of Naval Architecture, Ocean and Marine Engineering, University of Strathclyde, Glasgow, United Kingdom
4. Technology for Advanced Offshore Solutions, Edinburgh, United Kingdom
5. Newcastle Marine Services, Newcastle Upon Tyne, United Kingdom

ABSTRACT

The operation and maintenance (O&M) of an offshore wind turbine consumes large percentage of cost in the whole life of the offshore wind project. In most maintenance strategies, the service operation vessels (SOV) are widely employed in the maintenance activities. So far, the SOVs are large vessels to satisfy the requirement of equipment and functions. Some regular inspections for the wind farm are carried out by remotely operated underwater vessels (ROV). The offshore support vessel can be smaller in regular inspections. An attempt of small service operation vessel with ROV operating regular inspections is discussed in present research. The single point mooring method between offshore wind turbine and offshore support vessel is applied in the case. The relative distance between the vessel and the tension in the connecting lines are discussed under different environmental conditions. The numerical results are validated by the full-scale measurements on the vessel. It is found that the tension in the connecting lines is highly determined by the wind and wave directions. The wind-wave misalignments are also considered in the present study. It is found that the wind-wave misalignment may lead the sharp increase of relative distance and tension in connecting lines between offshore wind turbine and support vessel.

.

Keywords: Offshore wind turbine; Maintenance; Support vessel

NOMENCLATURE

$\Phi(\boldsymbol{X}, t)$	Total velocity potential
$\Phi^{(1)}(\boldsymbol{X}, t)$	Total first-order velocity potential
ω	Circular frequency of incident wave
$\phi^{(1)}(\boldsymbol{X})$	Complex amplitude of the first-order velocity potential
$\phi_I^{(1)}$	Complex amplitude of the first-order incident wave potential
$\phi_D^{(1)}$	Complex amplitude of the first-order diffraction wave potential
$\phi_R^{(1)}$	Complex amplitude of the first-order radiation wave potential
$\xi_m^{(1)}$	Complex amplitude of the first-order oscillatory motion
$\phi_m^{(1)}$	First-order unit-amplitude radiation potential in mode m
m	Modes referred to as surge, sway, heave, roll, pitch and yaw
n_m	m^{th} component of the normal vectors
k	Wavenumber
ϕ_{ij}^+	Sum-frequency time-independent velocity potential
ϕ_{ij}^-	Difference-frequency time-independent velocity potential
$\phi_I^{\pm}$	Second-order time-independent incident wave potential

$\phi_D^{\pm}$ Second-order time-independent diffraction wave potential

INTRODUCTION

In response to the global warming, the development of the renewable energy is speeding up. Offshore wind as an abundant green energy source is paid much attention in recent years. Several governments announced their offshore wind plans. The UK government confirmed that the offshore wind will produce more than enough electricity to power every home in country by 2030 which will reach 40GW [1]. USA announced 30GW of offshore wind power which will require the installation of 2000 turbines in water by 2030 [2]. China also states over 45GW offshore wind capacity plan in its 14th "Five-year-plan". The Strategy of the EU proposes to increase Europe's offshore wind capacity from its current level of 12 GW to at least 60 GW by 2030 [3].

With the large increased number of the installation of the offshore wind projects all over the world, the operation and maintenance (O&M) for the wind farm attract more attention than before. Based on the estimations of Carroll et al. [4], Johnston et al. [5] and D Fraile F Selot [6], the cost of O&M takes 20-25% of the levelized cost of energy (LCOE), which represents the average life-cycle cost of the electricity generated from a given power source per megawatt-hour. During the maintenance period, services are always operated by large ocean engineering service operation vessels (SOV). However, the consumption of traditional large SOVs is very high. There are several research on the O&M strategies to optimises maintenance plan like path, scheduling and operation window selection. Dai et al. [7] proposed the concept of "maintenance grouping" making different kinds of tasks mix in same planning period or visit. The overall cost of the maintenance was reduced by Lazakis and Khan [8] by optimizing the whole maintenance task sequence of the wind farm.

Some kinds of maintenance require the support vessel to stay by the turbine during the operation period. Some investigations about SOVs are necessary. Li [9] investigated the strength of bridge between wind turbine and SOV. Endrerud et al. [10] introduced a new concept of crew transfer vessel to replace the SOV as accommodation during the operation period. Some regular inspection maintenance is also carried by the SOVs using remotely operated underwater vessel (ROV). However, the large ocean engineering vessels applied in the operation cost approximately five to ten times of small vessels in the regular inspection maintenance. In other words, the application of a small support vessel can decrease the cost of O&M for offshore wind farm significantly.

A new mooring method that single point mooring system (SPMS) is developed for the small offshore support vessel which can significantly cut the complexity and cost of conducting sub-sea inspection and maintenance operations of the offshore wind farm. With the SPMS, the vessel achieves a stable position under the wind, wave, and current forces by utilising a single rope/mooring line to restrain motion at a fixed radius around the offshore wind turbine foundation. The new mooring method is similar to the single point mooring system which are widely applied in the offshore engineering for oil and gas [11,12 and 13].

In the present study, the relative distance between vessel and the wind turbine is calculated based on the linear analysis and nonlinear analysis. The hydrodynamic interaction between wind turbine tower and the support vessel is ignored due to the large distance between two bodies.

METHODOLOGY

The present study is carried out based on the potential theory. The fluid is assumed as ideal without viscosity, irrotational and incompressible. The incident wave is assumed as small slope wave which can be perturbated into Stokes wave profile.

The total first-order velocity potential $\Phi^{(1)}(\boldsymbol{X}, t)$ for the wave-body interaction can be expressed by a sum of components having circular frequency ω:

$$\Phi^{(1)}(\boldsymbol{X}, t) = Re\{\phi^{(1)}(\boldsymbol{X})e^{-i\omega t}\}$$

$$= Re\left\{\left[\phi_I^{(1)} + \phi_D^{(1)} - i\omega \sum_{m=1}^{6} \xi_m \phi_m\right] e^{-i\omega t}\right\}$$

$$(1)$$

Here the $\phi^{(1)}(\boldsymbol{X})$ is the complex first-order velocity potential which is independent of time. The $\phi^{(1)}(\boldsymbol{X})$ can be decomposed to the sum of incident wave potential $\phi_I^{(1)}$, diffraction potential $\phi_D^{(1)}$, and radiation potential $\phi_R^{(1)}$[14].

The first-order incident wave spatial potential $\phi_I^{(1)}$ can be expressed as:

$$\phi_I^{(1)} = \frac{-igA}{\omega} \frac{\cosh k(z+h)}{\cosh kh} e^{ikx} \qquad (2)$$

The radiation potential is a linear combination of the modes of motion components:

$$\phi_R^{(1)} = -i\omega \sum_{m=1}^{6} \xi_m \phi_m \qquad (3)$$

ξ_m is the first-order complex amplitude of the oscillatory motion in mode of body in m-th DOF. ϕ_m is the first-order unit-amplitude radiation potential (specifically, unit amplitude means the unit-amplitude linear or angular velocity of the rigid body motion). These modes are referred to as surge, sway, heave, roll, pitch and yaw in the increasing order of m.

Both first-order radiation can be achieved based by the solution of BVPs:

$$\nabla^2 \phi_m = 0 \qquad \text{in fluid domain} \quad (4)$$

$$-\omega^2 \phi_m + g \frac{\partial \phi_m}{\partial z} = 0 \qquad \text{at free surface} \quad (5)$$

$$\frac{\partial \phi_m}{\partial z} = 0 \qquad \text{at sea bottom} \quad (6)$$

$$\frac{\partial \phi_m}{\partial n} = n_m \qquad (7)$$

$$\lim_{R \to \infty} \sqrt{R}\left(\frac{\partial \phi_m}{\partial R} - ik\phi_m\right) = 0 \qquad \text{in far field} \quad (8)$$

where $R = \sqrt{x^2 + y^2 + z^2}$, n_m is generalized normal vectors.

$$n_m = \begin{cases} \vec{n} & m = 1,2,3 \\ (x, y, z) \times \vec{n} & m = 4,5,6 \end{cases} \qquad (9)$$

$\vec{n}$ is the unit normal vector pointing towards the body surface, (x, y, z) is the position vector on body surface. The first-order diffraction potential also satisfies the Laplace equation and similar boundary conditions.

The drift motion of vessel is considered in the present study. The second-order velocity potential is also solved by the solution of BVPs:

$$\nabla^2 \phi_D^\pm = 0 \qquad \text{in fluid domain} \qquad (10)$$

$$-(\omega_i \pm \omega_j)^2 \phi_D^\pm + g \frac{\partial \phi_D^\pm}{\partial z} = Q_F^\pm \quad \text{at free surface} \quad (11)$$

$$\frac{\partial \phi_D^\pm}{\partial z} = 0 \qquad \text{at sea bottom} \qquad (12)$$

$$\frac{\partial \phi_D^\pm}{\partial n} = Q_B^\pm \qquad \text{on mean wet surface of vessel} \quad (13)$$

$$\lim_{R \to \infty} \sqrt{R} \left(\frac{\partial \phi_D^\pm}{\partial R} - ik\phi_D^\pm \right) = 0 \qquad \text{in far field} \qquad (14)$$

As in the first-order, the second-order velocity potential can be decomposed into three components, the second-order incident wave potential $\phi_I^\pm$, the second-order diffracting wave potential $\phi_D^\pm$ and the second-order radiation potential $\phi_R^\pm$. $Q_F^\pm$ and $Q_B^\pm$ are the surface and body forcing terms [14].

The second-order sum- and difference-frequency components of the incident potentials $\phi_I^\pm$ can be expressed as:

$$\phi_I^+(x) = \frac{1}{2}(q_{ij}^+ + q_{ji}^+) \frac{\cosh k^+(z+h)}{\cosh k^+ h} e^{ik^+ x} \qquad (15)$$

$$\phi_I^-(x) = \frac{1}{2}(q_{ij}^- + q_{ji}^{-*}) \frac{\cosh k^-(z+h)}{\cosh k^- h} e^{ik^- x} \qquad (16)$$

where $k^\pm = k_i \pm k_j$ is the wavenumber and

$$q_{ij}^+ = -\frac{ig A_i A_j}{2\omega_i} \frac{k_i^2 - v_i^2 + 2k_i k_j - 2v_i v_j}{v^+ - k^+ \tanh k^+ h} \qquad (17)$$

$$q_{ij}^- = -\frac{ig A_i A_j^*}{2\omega_i} \frac{k_i^2 - v_i^2 - 2k_i k_j - 2v_i v_j}{v^- - k^- \tanh k^- h} \qquad (18)$$

where $v^\pm = \frac{(\omega_i \pm \omega_j)^2}{g}$

It is noted that the radiation describes the disturbance due to the second-order motion of the body and it is linearly proportional to the motion amplitude [15]. i is the imaginary unit.

$$\phi_R^\pm = -i(\omega_i \pm \omega_j) \sum_{k=1}^{6} \left(\xi_m^{(2)} \phi_m^{(2)} \right) \qquad (19)$$

$\xi_m^{(2)}$ is the second-order complex amplitude of the oscillatory motion in mode of body m-th DOF. $\phi_m^{(2)}$ is the second-order unit-amplitude radiation potential (specifically, unit amplitude means the unit-amplitude linear or angular velocity of the rigid body motion).

MODEL SET-UP OF THE OFFSHORE WIND TURBINE AND OFFSHORE SUPPORT VESSEL

Offshore support vessel

The offshore support vessel employed in the study is a industry service vessel. The main particulars of the vessel are shown in Table 1.

Table 1 Particulars of offshore support vessel

Dimensions	Unit	Value
Length overall	m	38.92
Length	m	32.10
Length waterline	m	34.60
Breadth Moulded	m	9.20
Depth Moulded	m	4.50
Draught	m	3.10
Displacement	m³	495.0
LCG from AP (After perpendicular)	m	15.47
VCG from BL (Base line)	m	4.25
Mass	ton	393

Fixed offshore wind turbine

To simplify the problem of the maintenance operation process simulated, this study has modelled a mono-pile bottom fixed wind turbine. The fixed wind turbine Siemens SWT-3.6-120 Offshore with a tripod support structure is considered as a fixed offshore wind turbine for this project (Figure 1). The height of the tower is set to be 120m and the diameter of the column of the support structure is 6.5m. The hight of the supporting structure is 35m. The widest part of tower's diameter is 6m. Further details are shown in Table 2. The floating wind turbine is considered as OC3 Spar type offshore wind turbine (Figure 2).
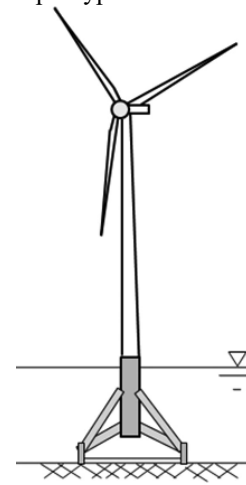
Figure 1 Configuration of fixed offshore wind turbine [17]
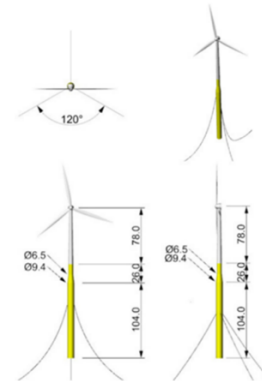
Figure 2 Configuration of OC3 Spar-type floating offshore wind turbine

Table 2 Particulars of offshore wind turbine

Dimensions	Unit	Value
Depth to Platform Base Below WL (Total Draft)	m	35
Height of Tower	m	120
Elevation to Platform Top (Tower Base) Above WL	m	10
Depth to Top of Taper Below WL	m	4
Depth to Bottom of Taper Below WL	m	12
Platform Diameter Above Taper	m	6.5
Platform Diameter Below Taper	m	9.4

Connecting mooring system

The single rope/mooring line to restrain motion of the vessel at a fixed radius around the foundation is a 3-strand Superflex polyester rope with dimension of 24 mm which is the same as used in the vessel. The MBL (Minimum Breaking Limitation) of the mooring rope is 10 tonnes. The load vs elongation of the mooring line shows in Table 3.

Table 3 The load vs Elongation of the mooring line

Elongation (%)	Force (N)
0.049	318.19
0.075	3210.88
0.100	10081.04
0.122	19482.25
0.138	30329.86
0.155	50940.26
0.163	66850.11
0.167	78782.44
0.183	89268.48
0.189	100116.09
0.195	108432.59
0.199	111686.85

In the field operation, one end of the mooring line is secured to the bollard at deck, then the mooring line bypasses the turbine structure and the other end of the mooring line is attached to the fixed dynamometer to vessel structure for reading the tension. The vessel and the mooring are a passive system. There is no winch force just a maximum load on the system based on the load cell and mooring line specification. As the ship mooring system is passive, there is no rated pull force. During the operation, the vessel is moving around the wind turbine since there is a connecting line's restriction.

To simplify the modelling aimed at reducing computational timing, the connection between offshore support vessel and wind turbine are simplified in the present project into two lines which are attached to same point in the middle of the wind turbine's structure and two separate fairleads on offshore support vessel. The fixed wind turbine is also simplified into a cylinder with a constant force at the head of the cylinder which represents the wind force on the turbines. Since the distance between the two structures are very large, the hydrodynamic interaction is ignored in the present study.

INTERACTION BETWEEN OFFSHORE WIND TURBINE AND OFFSHORE SUPPORT VESSEL

Full scale test and numerical simulation environment condition

Several simulations of representative weather conditions for North Sea locations are verified in order to calibrate the model with measured test data from the inspection campaign which was taken place across a number of offshore wind farms in 2020. The data collection is carried out at a large number of offshore structures with different support structure design which assisted in data analysis and validation of the numerical system, as well as any optimisations applied at full scale.

The environmental data are collected from weather forecast for the wind farm. By selecting four offshore wind turbines from the field, selecting the environmental conditions for the exact time while the vessel hang to the specific turbine (Table 4).

Table 4 Environmental data collected from the weather forecast

		Case #26	Case #72
Wind	Direction (deg)	NW/150	NW/125
	Value (m/s)	2.4-3.6	3.6-7.9
Wave	Direction (deg)	NW/150	NW/125
	Value (m)	0.2	0.5
Swell	Direction (deg)	SE/220	SW/250
	Value (m)	0.2	0.2
Current	Direction (deg)	NW/125	SE/325
	Value (m/s)	0.07-0.15	0.14-0.22

Mesh convergence of the offshore support vessel model

Since there are two bodies in the hydrodynamic interaction calculation in the present study, the panel mesh for wind turbine and vessel are needed. The wind turbine and support vessel are analysed separately. The hydrodynamic parameters are calculated for the two structures connected by the SPMS. Mesh convergence analysis is conducted in the present study as shown in Figure 3. The panel mesh model is shown in Figure 4(a) and the simplified numerical model for whole system is shown in Figure 4(b).
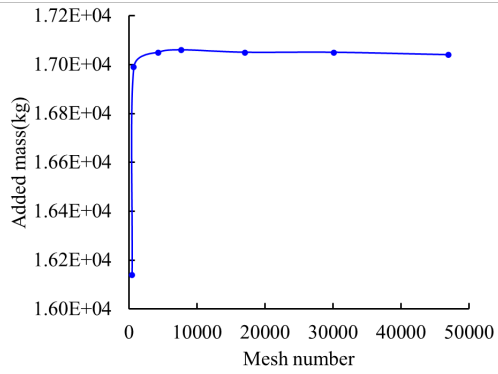
(a) Surge added mass of offshore support vessel
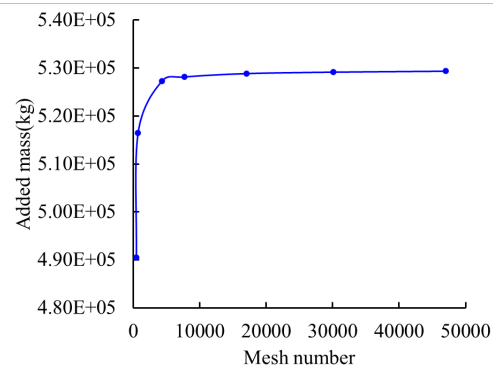
(b) Heave added mass of offshore support vessel
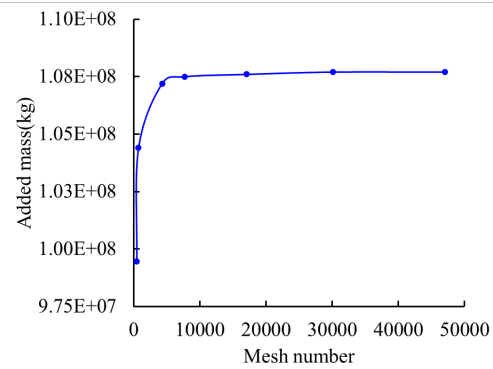
(c) Roll added mass of offshore support vessel
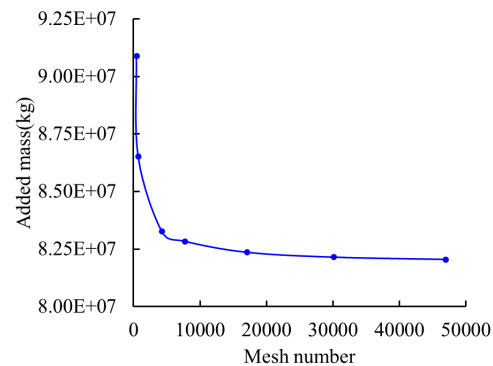
(d)Yaw added mass of offshore support vessel

Figure 3 Mesh convergence of offshore support vessel panel model.

The wind turbine has been simplified to a simple cylinder, so it is very easy to reach the convergence with increasing panel meshes. Once the panel mesh of offshore support vessel reaches the convergence, the meshes of wind turbine and vessel panel model can be determined.

(a)

(b)
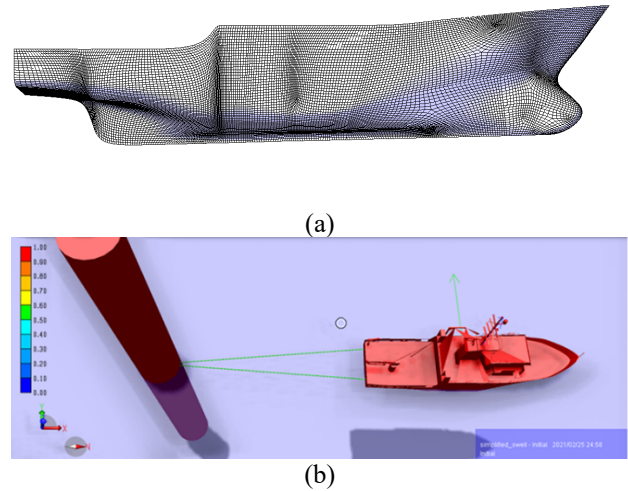
Figure 4 (a):Visualization of the panel mesh of offshore support vessel; (b): Simplified numerical model of the whole system.

The added mass in different direction for offshore support vessel with different meshes are calculated and shown in Figure 3. The added mass in surge, heave and roll direction converged very fast with increasing mesh number. The added mass in yaw direction is the most difficult hydrodynamic parameter to reach convergence with the increasing mesh number. When the mesh number is larger than 20000, the added mass converged in all direction.

Validation of the force along the connecting lines
The numerical model setting up by SIMA is further validated by comparison with the full-scale measurements obtained from operation at sea during offshore wind farm services. The environmental information of wind and current is applied in the simulation. The detailed environmental condition is shown in Table 4. The maximum and mean tension in the mooring lines between offshore support vessel and wind turbine (Figure 5) are applied to validate the accuracy of the numerical simulation in this chapter. The wind and current force are calculated using the wind and current coefficient. The coefficients are estimate using a similar shape vessel's coefficient. In the numerical simulation, the wind and current force are simplified as constant forces.
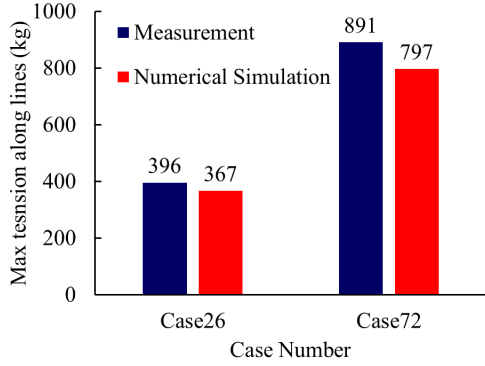
(a) Maximum tension along connecting mooring lines
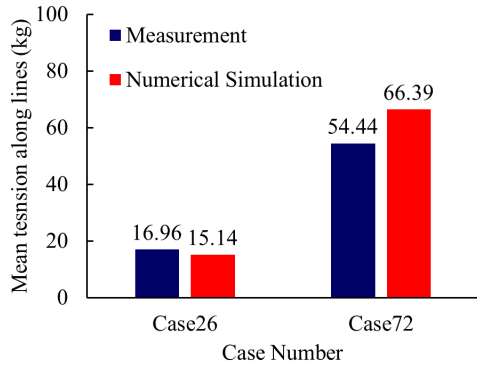
(b) Mean tension along connecting mooring lines

Figure 5 Maximum and mean tension along the connecting mooring lines between wind turbine and offshore support vessel

Two sets of environmental conditions are employed in the simulation and with the full-scale results. The wind and current velocity are adjusted in the range given in Table 4. According to Figure 5, both maximum tension and mean tension along the connecting mooring lines between wind turbine and offshore support vessel under two conditions obtained from numerical simulation and full-scale measurements are similar. In Figure 5, the duration of the two full-scale condition Case 26 and Case 72 lasted about 11 hours and 15 hours. The numerical simulation is operated as 3 hours. The difference of maximum and mean force along connecting lines in Case 72 are slightly larger than those in Case 26. The difference may be caused by the wind and current coefficients of offshore support vessel since the wind and current coefficients are estimated by a vessel which is similar to the offshore support vessel in the present study. Comparisons show that discrepancies between the present numerical solutions and the field measurements are approximately 7.3% for maximum tension and 10.7% for mean tension in the connecting mooring lines in Case 26 and 10.5% for maximum tension and 20.1%for mean tension in connecting lines in Case 72.

RESULTS AND DISCUSSION

Relative distance between the wind turbine and offshore support vessel and dynamic tension in the connecting mooring line

The vessel is tied to the wind turbine during the operation. The motion of the offshore vessel is restricted by the mooring lines between the vessel and wind turbine. In this chapter, there are 3 conditions (Table 5) are considered to investigate the motion characteristics of the offshore support vessel connected to the wind turbine during operation. The directions of the wave and current are set at the same direction from 0°. The difference between wind and wave direction is set from 0° to 30° which covers 95% of wind-wave difference range at sea [16]. Both fixed and floating offshore wind turbine are employed in the numerical simulation. The distance between centre of the supporting column of the wind turbine and the centre of vessel at original position is 56.5m.

Table 5 Environmental conditions applied in the numerical simulation

Environmental condition	LC	MC	HC
Wind speed (m/s)	3.4	5.4	7.9
Significant wave height (m)	0.4	0.8	1.3
Peak wave period (s)	4.5	5.5	6.5
Current velocity (m/s)	0.5	0.75	0.75

The motion of the offshore vessel and the force along the mooring lines connecting them are calculated using the present numerical model. The environmental conditions are increasing from low condition (LC) to high condition (HC) with increasing wave, wind and current speed.
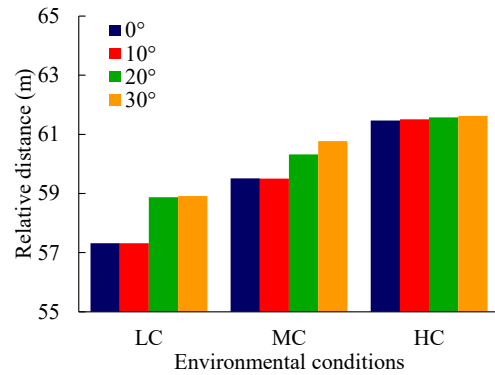
Figure 6 Maximum relative distance between fixed wind turbine and offshore support vessel under different environmental conditions and wind-wave misalignment

6
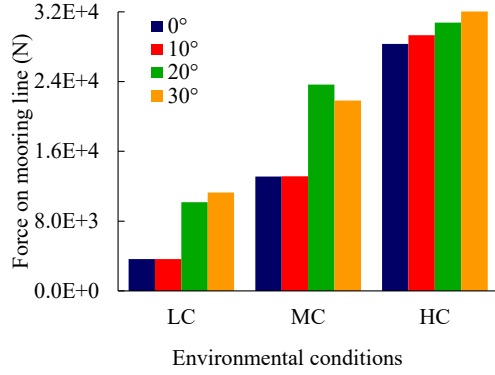
Figure 7 Maximum tension in the mooring lines between fixed wind turbine and offshore support vessel under different environmental conditions and wind-wave misalignment

Figure 6 shows the relative distance between the centre of the fixed wind turbine and offshore support vessel. It can be seen that the relative distance changes little when the misalignment is small (0° and 10°) under LC and MC conditions. However, with the misalignment increasing from 10° to 20°, the distance rises sharply and keeps in a stable level with increasing misalignment from 20° to 30°. When the environmental condition is high, the wind-wave misalignment has little impact on the relative distance as shown in Figure 6. It indicates that the wind direction is more dominant effect when the environmental condition is low. While the impact of the wind-wave misalignment on the relative distance is obvious in the range between 10° to 20°, it is less so for other misalignment range. This may depend on the wind force component comparing to the total environmental load. Under low environmental condition (e.g., 1.5 m/s), both wave and wind impact are small which results in the weak impact of the misalignment. As evident in Figure 8 and Figure 9, under high environmental condition (HC), the wind-wave misalignment is less dominant compared to low environmental condition (LC) and medium environmental condition (MC). Consequently, the critical value of wind-wave misalignment for the distinct jump of relative distance and tension in the connecting lines will change with wind strength as shown in Figure 8 and Figure 9. In this study, the LC condition is selected for further investigation with different wind speed.
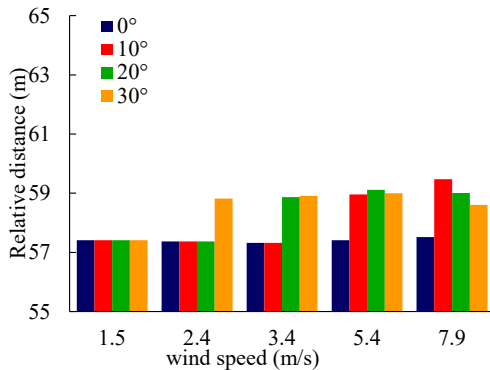
Figure 8 Maximum relative distance between fixed wind turbine and offshore support vessel under LC condition with different wind speed and wind-wave misalignment
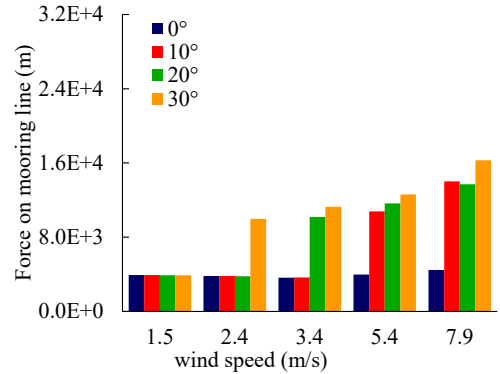
Figure 9 Maximum tension in mooring line between fixed wind turbine and offshore support vessel under LC condition with different wind speed and wind-wave misalignment

The relative distance and tension in the connecting mooring line between wind turbine and offshore support vessel under different wind speeds are shown in Figure 8 and Figure 9 respectively. The wave condition and current speeds are set as constant which is same to the LC condition. The direction of wind and current are also set from 0°. It is noted that a critical value of wind-wave misalignment which leads the distinct jump of relative distance and tension in the connecting line is changing from more than 30° to less than 10° with increasing wind speed from 1.5m/s to 7.9m/s. The critical value of wind-wave misalignment is given approximately due to the limitation of the cases with different misalignments considered in the study. For instance, at wind speed 2.4 m/s, a clear jump is observed for a critical value of wind-wave misalignment approximately 30°. However, the impact of wind-wave misalignment on the relative motion and the tension in the connecting line are rather small before and after the critical value. This verified that the sudden jump of the relative distance and tension in the connecting mooring line is the consequence of the combined effect of the wind strength and the wind-wave misalignment. It also indicates that the wind-wave misalignment needs to be considered during field operation.

The relative distance and tension the mooring line are calculated under the conditions that the base direction (wave direction) is 0° and wind direction is changing from 0° to 30°. It is worth noting that during the offshore support vessel operation at sea, the base direction is random. The relative distance and the tension in connecting line under different base direction and wind-wave misalignment are further investigated in detail.
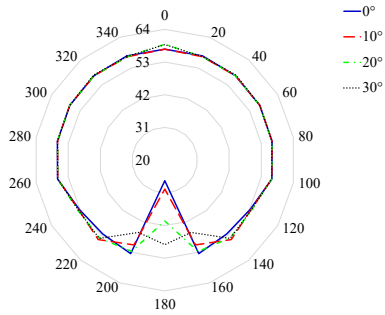
(a) Max. relative distance between vessel and wind turbine (*m*)
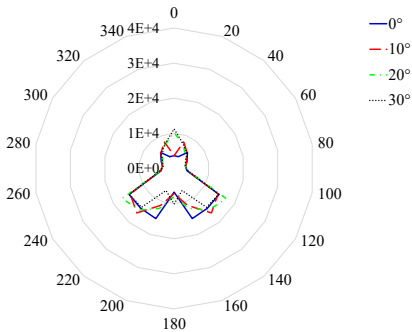
(b) Max. tension in connecting line (*N*)

Figure 10 Maximum relative distance and maximum tension in the connecting mooring line (b) under the LC condition with different wind-wave misalignment
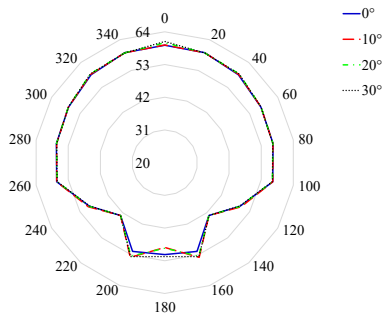
(a) Max. relative distance between vessel and wind turbine (*m*)
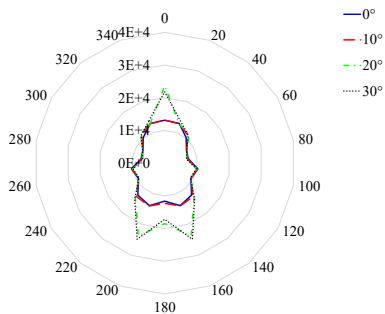
(b) Max. tension in connecting line (*N*)

Figure 11 Maximum relative distance and maximum tension in the connecting mooring line (right) under the MC condition with different wind-wave misalignment
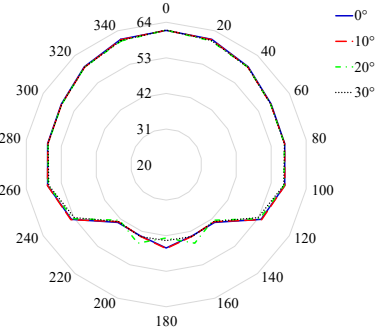
(a) Max. relative distance between vessel and wind turbine (*m*)
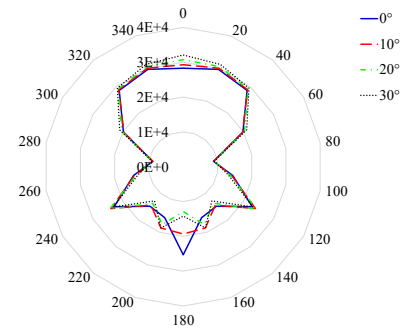
(b) Max. tension in connecting line (*N*)

Figure 12 Maximum relative distance and maximum tension in the connecting mooring line (right) under the HC condition with different wind-wave misalignment

The maximum relative distance and the maximum tension in the connecting mooring line under different environmental conditions with different wind-wave misalignment are shown in Figure 10-12. The base directions (incident wave direction) are selected from 0° to 180°. Since the coupled wind turbine-vessel model is symmetrical, the relative distance and the tension curves are also symmetrical. For all environmental conditions (LC, MC, HC), it is seen that the misalignment has significant and varied impact on both relative distance and tension in the connecting lines when the base direction is around 0° and 180°. However, for the base direction in the range of 60° to 120°, the relative distance and the tension in the connecting lines are similar under different wind-wave misalignments as the four lines of different colours representing the four misalignments overlap. Since the projection of the coupled model changes little in the direction ranging from 60° to 120°, the wind force only changes slightly leading to the smaller difference of relative distance and tension in the connecting line under different wind-wave misalignment.

Dynamics analysis of coupled system of floating wind turbine and offshore support vessel

The analysis between floating wind turbine and the offshore support vessel is also carried out in the present study. The floating wind turbine is using the OC3 spar-type structure as shown in Figure 2. The operation conditions in the simulation are same with the fixed wind turbine.

There is a clear trend of offshore wind development progressively moving towards further offshore due to the increased wind energy density. Prototypes of floating offshore wind turbines were recently installed and connected to local grid, and a number of large-scale wind farms with floating offshore wind turbines are proposed around the world. This section presents a hydrodynamic study of coupled system of floating wind turbine and offshore support vessel representing the real-world offshore wind farm service operation.

The maximum relative distance and the maximum tension in the connecting lines between floating wind turbine and offshore support vessel are calculated to investigate the impact due to the motion of the floating wind turbine on the maximum relative distance and the maximum tension in the connecting line.

Figure 13 shows that the relative distance between the floating wind turbine and the offshore support vessel decreases as the misalignment increases for the low environmental condition (LC) applied. However, the misalignment appears to have little impact on the relative distance for the medium and high environmental conditions (MC and HC) considered in the simulation. It indicates that the maximum relative distance is more sensitive to the wind-wave misalignment at low environmental condition.

Comparing to the coupled system of a fixed wind turbine and offshore support vessel, Figure 14 shows that the wind-wave misalignment has greater impact on the maximum tension in the connecting line under the low environmental condition (LC) and the tension tends to decrease as the misalignment increases. In contrast to that, the misalignment of wind-wave appears to have little impact on the higher environmental conditions (MC and HC).

The maximum relative distance and the maximum line tension with different wind speed under LC condition for wave and current are calculated to examine the details of the wind impact. The wind speed is set from 1.5 m/s to 7.9 m/s (with the original wind speed is 3.4 m/s) and four wind-wave misalignments (0°, 10°, 20° and 30°) are considered.
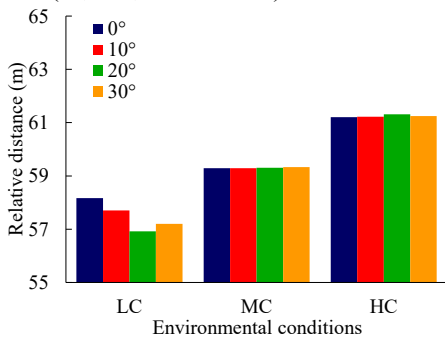
Figure 13 Maximum relative distance between floating wind turbine and offshore support vessel under different environmental conditions and wind-wave misalignment
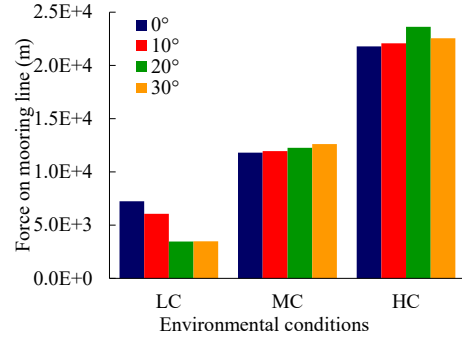
Figure 14 Maximum force along the mooring lines between floating wind turbine and offshore support vessel under different environmental conditions and wind-wave misalignment
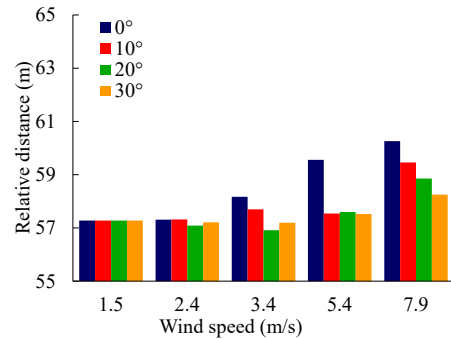
Figure 15 Maximum relative distance between floating wind turbine and offshore support vessel under LC condition with different wind speed and wind-wave misalignment
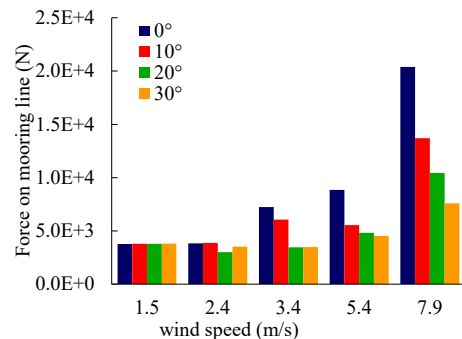
Figure 16 Maximum force along mooring lines between floating wind turbine and offshore support vessel under LC condition with different wind speed and wind-wave misalignment

Figure 15 and Figure 16 shown the maximum relative distance and the maximum tension in the connecting line respectively. It is noted that the maximum relative distance and the maximum line tension are of similar trend when the wind speed is low (1.5m/s and 2.4m/s). Both wind speed and wind-wave misalignment appear to have little impact on the maximum relative distance and the maximum line tension. As the wind speed increases, the maximum relative distance and the maximum line tension tend to increase. It is evident that the maximum relative distance and the maximum line tension decrease markedly with increasing wind-wave misalignment

under wind speed from 3.4 m/s to 7.9 m/s showing greater impact of wind-wave alignment at higher wind speed. Different to the fixed wind turbine, this characteristic indicates that the maximum line tension occurs when the wind, wave and current are in the same direction (colinear environment), an important information for the on-board crew of the offshore support vessel during the service operation of the floating wind turbines.

CONCLUSION

The coupled system of a fixed or floating wind turbine and an offshore support vessel under different environmental conditions and various wind-wave misalignment are investigated based on numerical simulation. The present numerical model for the coupled analysis in time domain are rigorously validated against field measurements of the full-scale operation at sea during the service to offshore wind farms located in Baltic Sea and North Sea. The maximum relative distance and the maximum tension in the connecting lines are examined in detail under different conditions.

- When the wind turbine is fixed, the maximum relative distance and force along the connecting lines are significantly influenced by the wind-wave misalignment under the low condition (LC) and medium condition (MC). However, there is little impact of misalignment on these under high condition (HC).
- The increasing wind speed and wind-wave misalignment leads to a jump of maximum relative distance and maximum force along the connecting lines when the wind turbine is fixed.
- When the wind turbine is fixed, the impact of the wind-wave misalignment on the relative distance and force are mostly concentrated in the base directions of 0° and 180°. When the base direction is at the range of 60° to 120°, the relative distance and force along connecting lines are similar under different wind-wave misalignments.
- When the wind turbine is floating, the impact of the wind on maximum relative distance and force along the connecting lines are shown under low condition. There is little impact of wind-wave misalignment when the environmental condition is medium and high condition.

ACKNOWLEDGEMENTS

REFERENCES

[1] Adnan Durakovic, 2021, UK Prime Minister: Offshore Wind to Power Every Home by 2030, OffshoreWind.biz

[2] Sonal Patel, 2021, Biden Administration Sets National 30-GW Offshore Wind Target, POWER

[3] European Commission, 2021, Boosting Offshore Renewable Energy for a Climate Neutral Europe, European Commission - Press release

[4] Carroll, J., Mcdonald, A. & Mcmillan, D. 2016. Failure rate, repair time and unscheduled O&M cost analysis of offshore wind turbines. Wind Energy, 19, 1107-1119.

[5] Johnston, B., Foley, A., Doran, J. & Littler, T. 2020. Levelised cost of energy, A challenge for offshore wind. Renewable Energy, 160, 876-885.

[6] Selot, F., Brindley, G. & Walsh, C. 2019. Offshore wind in europe–key trends and statistics 2018.

[7] Dai, L., Stålhane, M. & Utne, I. B. 2015. Routing and scheduling of maintenance fleet for offshore wind farms. Wind Engineering, 39, 15-30.

[8] Lazakis, I. & Khan, S. 2021. An optimization framework for daily route planning and scheduling of maintenance vessel activities in offshore wind farms. Ocean Engineering, 225, 108752.

[9] Li, B. 2020. Multi-body hydrodynamic resonance and shielding effect of vessels parallel and nonparallel side-by-side. Ocean Engineering, 218, 108188.

[10] Endrerud, V., Austreng, K. R., Keseric, N. & Liyanage, J. P. New vessel concepts for operations and maintenance of offshore wind farms. The Twenty-fifth International Ocean and Polar Engineering Conference, 2015. OnePetro.

[11] Wu, W., Wang, Y., Tang, D., Yue, Q., Du, Y., Fan, Z., ... & Zhang, Y. 2016. Design, implementation and analysis of full coupled monitoring system of FPSO with soft yoke mooring system. Ocean engineering, *113*, 255-263.

[12] Ma, Y., Hu, Z., Qu, Y., & Lu, G. 2013. Research on the characteristics and fundamental mechanism of a newly discovered phenomenon of a single moored FPSO in the South China Sea. Ocean engineering, *59*, 274-284.

[13] Liu, Y., Yoshida, S., Yamamoto, H., Toyofuku, A., He, G., & Yang, S. 2018. Response characteristics of the DeepCwind floating wind turbine moored by a single-point mooring system. Applied Sciences, *8*(11), 2306.

[14] Kim, M.-H. & Yue, D. K. 1989. The complete second-order diffraction solution for an axisymmetric body Part 1. Monochromatic incident waves. Journal of Fluid Mechanics, 200, 235-264.

[15] Newman, J. N. 1974. Second-order, slowly-varying forces on vessels in irregular waves.

[16] Bachynski, E. E., Kvittem, M. I., Luan, C. & Moan, T. 2014. Wind-wave misalignment effects on floating wind turbines: motions and tower load effects. Journal of Offshore Mechanics and Arctic Engineering, 136

[17] Thakur, S., Abhinav, K. & Saha, N. 2018. Load mitigation using slotted flaps in offshore wind turbines. Journal of Offshore Mechanics and Arctic Engineering, 140(6).